19th Australasian Fluid Mechanics Conference
Melbourne, Australia
8-11 December 2014

Three-dimensional Linear Stability Analysis of the Flow Around a Sharp 180^o Bend

A. M. Sapardi[1,2], W. K. Hussam[1], A. Pothérat[3] and G. J. Sheard[1]

[1]The Sheard Lab, Department of Mechanical and Aerospace Engineering, Monash University, Victoria 3800, Australia

[2]Department of Mechanical Engineering, International Islamic University Malaysia, Kuala Lumpur 53300, Malaysia

[3]Applied Mathematics Research Centre, Coventry University, Coventry CV1 5FB, United Kingdom

Abstract

This study seeks to characterise the stability of a two-dimensional channel flow involving a 180-degree sharp bend, to infinitesimal three-dimensional disturbances by way of a linear stability analysis. A highly accurate global linear stability analysis of the flow is presented via the Reynolds number Re varies in the range $100 \leq Re \leq 700$, this Re range produces steady-state two-dimensional flow solutions for bend opening ratio (ratio of bend width on inlet height) $\beta = 1$. The two-dimensional base flow solutions demonstrate that as β decreases, the transition from steady to unsteady occurs at lower Reynolds number. The stability analysis shows that the flow first becomes unstable to a synchronous three-dimensional instability mode with spanwise wavenumber $k = 2$ at approximately $Re = 400$, whereas the two-dimensional solution branch undergoes transition to unsteady flow somewhere near $Re \approx 800$. Instability mode structures associated with the leading eigenvalues are localized at the re-attachment point of the first separation bubble and the separation point of the second separation bubble. The stability analysis is used to produce neutral stability curves, and visualisations of the global modes of the system for typical Reynolds number are also presented.

Introduction

An important geometric feature of the ductwork carrying liquid-metal coolant fluid within prototype blankets in magnetic confinement fusion reactors is sharp 180-degree bends. The flow around the bend and the transport of heat from the far sidewall of the bend are critical aspects for the efficient transport of heat from the reactor for power generation [3]. Despite the relative simplicity of the geometry, the literature reveals a dearth of studies into this problem: the magnetohydrodynamic (MHD) problem has not previously been tackled, and consideration of the non-MHD case has received limited attention, with studies focusing only on the two-dimensional flow. The understanding of flow around a 180-degree bend in a channel was originally motivated by erosion and silt deposition around river bends [8], but it also underpins the duct flow problem with application to fusion reactor blankets.

Fundamentally, the two-dimensional flow creates recirculation structures that resemble those seen in several canonical confined flow problems, including the backward-facing step flow [1, 2]. The separated flow generated in both the 180-degree sharp bend geometry and the backward-facing step is due to a geometric perturbation caused by the sudden change in geometry. Flow separation caused by an abrupt geometry change is commonly observed in sharp river bends [7]. Specifically, the flow first passes over a large recirculation bubble attached to the downstream side of the inner corner of the bend, and subsequently a second recirculation bubble develops on the outer wall a little further downstream (Figure 1). Separating and reattaching flows play an important role in numerous engineering applications especially in heat transportation.

The aim of this paper is to quantify the critical flow transitions leading to turbulence in the flow around the sharp 180-degree bend. Numerous studies have elucidated the three-dimensional stability of backward-facing step flows and other confined flows, but not for flow in a 180-degree sharp bend.

Numerical Methodology

A viscous flow in a 180-degree sharp bend channel is investigated. The flow is assumed to be of constant density ρ and constant kinematic viscosity ν.

The fluid motion is governed by the incompressible Navier–Stokes equations, written in non-dimensional form as

$$\frac{\partial \mathbf{u}}{\partial t} = N(\mathbf{u}) - \nabla p + \frac{1}{Re}\nabla^2 \mathbf{u}, \tag{1}$$

$$\nabla \cdot \mathbf{u} = 0. \tag{2}$$

where $\mathbf{u}$ is the velocity field, p is the static pressure. The nonlinear advection term in convection form is taken as

$$N(\mathbf{u}) \equiv -(\mathbf{u} \cdot \nabla)\mathbf{u}. \tag{3}$$

Figure 1 illustrates the computational domain under consideration including the geometric parameters for the problem. The channel widths in the inlet and at the bend are represented by a and b, respectively. The height of the inlet and outlet are identical. The divider thickness is represented by c with d and e denoting the lengths of bottom and top boundaries. The ratio c/a is set to 0.04, while the lengths of the bottom and top boundaries determined by $(d-b)/a = 15$ and $e/d = 3$. The opening ratio of the bend is represented by $\beta = b/a$.

Fluid enters from the inlet and flows downstream past the sharp bend towards the outlet channel. The length of the outflow domain is sufficiently long to ensure that the results are independent of outflow effects. A convergence study determined acceptable outflow lengths between $20a \leq e-b \leq 100a$. The system is taken to be homogeneous in the spanwise direction and to

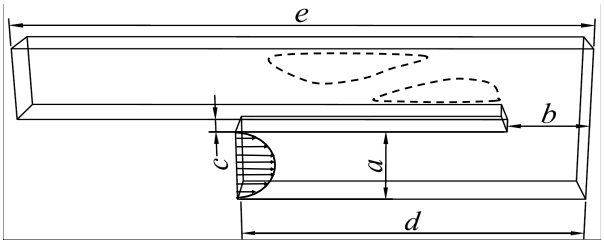

Figure 1. Flow geometry for the 180-degree sharp bend. Dashed lines indicate the location of the first (near the bend) and the second recirculation bubble (further downstream of the outlet).

be infinitely large in that direction by considering all spanwise Fourier modes.

Boundary conditions are imposed on the flows as follows. At the inflow boundary ($x = b - d, -1.02 \leq y \leq -0.02$), a Poiseuille velocity profile is imposed: $u_x = 1 - 4(y + 0.052)^2, u_y = 0, u_z = 0$. Due to viscosity, the velocity at the interface between the wall and the fluid, hence a no slip boundary condition ($\mathbf{u} = 0$) is imposed at the wall. At the outflow boundary ($x = b - e, 0.02 \leq y \leq 1.02$), a standard boundary condition for pressure ($p = 0$) is imposed.

In this study, we take $L_{\text{ref}} = a$, and $U_{\text{ref}} = U_o$, where a and U_o are inlet height and maximum inlet centerline velocity, respectively. Thus, the Reynolds number is defined as

$$Re \equiv \frac{U_o a}{\nu}. \tag{4}$$

Computational Methods

The governing equations are spatially discretised using a spectral-element method and time integrated using a third-order backward differentiation scheme [6]. The methods used to analyze linear stability of perturbations are based on time integration of the linearized Navier–Stokes equations. Velocity and pressure fields decomposed into a two-dimensional base flow and infinitesimal fluctuating disturbance components become:

$$\mathbf{u}(x,y,z,t) = \mathbf{U}(x,y,z,t) + \mathbf{u}'(x,y,z,t), \tag{5}$$

$$p(x,y,z,t) = P(x,y,z,t) + p'(x,y,z,t). \tag{6}$$

Substituting equations 5 and 6 into the Navier–Stokes equations (1,2), subtracting the base flow equations as well as disregarding the products of perturbation velocities results the linearised Navier–Stokes equations

$$\frac{\partial \mathbf{u}'}{\partial t} = -DN\mathbf{u}' - \nabla p' + \frac{1}{Re}\nabla^2 \mathbf{u}', \tag{7}$$

$$\nabla \cdot \mathbf{u}' = 0. \tag{8}$$

This set of equations describes the evolution of the perturbation field. Consequently, Re can be used to characterise the stability of a perturbation field $\mathbf{u}'$. The linearised advection term is defined as

$$DN\mathbf{u}' = (\mathbf{U} \cdot \nabla)\mathbf{u}' + (\mathbf{u}' \cdot \nabla)\mathbf{U}. \tag{9}$$

Since the flow is homogeneous in the spanwise direction, we can decompose general perturbations into Fourier modes with spanwise wavenumber

$$k = \frac{2\pi}{\lambda}, \tag{10}$$

where λ is the wavelength in the spanwise direction. As per equation (7,8), the equations are linear in $\mathbf{u}'$ and therefore the three-dimensional perturbation field forms are linearly independent, hence, in terms of numerical implementation, the perturbation field with different spanwise wavenumbers only couple with the base flow, meaning that the computation of each of them can be done independently.

$$\left\{ \begin{array}{c} u'(x,y,z,t) \\ v'(x,y,z,t) \\ w'(x,y,z,t) \\ p'(x,y,z,t) \end{array} \right\} = \left\{ \begin{array}{c} u'\cos(x,y,t)kz \\ v'\cos(x,y,t)kz \\ w'\sin(x,y,t)kz \\ p'\cos(x,y,t)kz \end{array} \right\}. \tag{11}$$

The behaviour of the stability has been reduced into Fourier components which comprises a two-parameter problem of Re and k.

Let $\mathscr{A}(\tau)$ represent the linear evolution operator over a time τ defined by equations 7 and 8

$$\mathbf{u}'(\tau) = \mathscr{A}(\tau)\mathbf{u}'(\tau). \tag{12}$$

An eigenvalue problem in terms of operator $\mathscr{A}(T)$ for flows with a time period T is obtained

$$\mathscr{A}(\tau)\hat{\mathbf{u}} = \mu\hat{\mathbf{u}}, \tag{13}$$

$$\mu \equiv e^{(\sigma + i\omega)T}, \tag{14}$$

where σ and ω, respectively, are the growth rate and angular frequency of a linear instability mode. Complex eigenvalue is denoted by μ and $\hat{\mathbf{u}}$ denotes the eigenvector field.

For steady base flows, T represents an arbitrary interval of time over which the instability mode evolved. The dominant eigenvalues μ determine the stability of the base flow. Such that the base flow is unstable if $|\mu| > 1$, and stable if $|\mu| < 1$. For $|\mu| = 1$, the flow is neutrally stable and represents a system in which infinitesimal perturbations will neither decay nor grow. The Reynolds number corresponding to $|\mu| = 1$ is considered as the critical Reynolds number for the onset of the instability.

Code Validation

A rigorous test of a code is one in which all aspects of the solver are exercised. The validation of the numerical computation has been done with several particular cases. There are several numerical studies have been done by previous researchers [4, 9] in analysing the structure of the flow in almost similar geometry. There are several results in these studies that can be used to validate current code to shows the aptness of this code to conduct this numerical study, such as length of recirculation bubble in the downstream channel and samples of contour of spanwise vorticity magnitude. Code is considered valid if it does not shows obvious contradictions with previous findings.

It is observed that the streamlines break away from the boundary when a boundary layer develops near the surface of an abrupt geometry change. The location of separation and reattachment points are located where the streamwise velocity is constant with respect to the transverse direction,

$$\left.\frac{\partial u}{\partial y}\right|_x = 0. \tag{15}$$

Figure 2 represents the comparison between the recirculation length of the first bubble (L_{R1}/a) in a steady-state flow ($Re < 800$) between present and previous results [9, 4]. The comparison displays a strong agreement between the studies. It is also shown that the length of recirculation bubble keeps increasing before it collapses due to the unsteadiness of the flow when $Re > 800$. The elongation of the recirculation bubble is linear until second recirculation bubble appears further downstream of the channel at $Re \approx 250$.

Test of Eigenvalue Computations

The precision of eigenvalue, μ and eigenmode $\hat{\mathbf{u}}$ produced by subspace iteration has been quantified by using the residual

$$r = \| \mathscr{A}\hat{\mathbf{u}} - \mu\hat{\mathbf{u}} \|, \tag{16}$$

where $\| \cdot \|$ is the standard vector norm and the eigenmodes are scaled such that $\| \hat{\mathbf{u}} \| = 1$. The linear stability analysis technique uses an iterative process to obtain the leading eigenvalues and eigemodes of the system. The process ceases when $r < 10^{-7}$ is achieved.

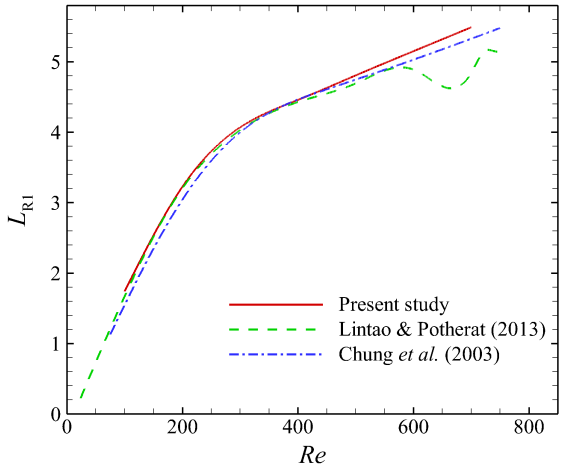

Figure 2. Validation of the first recirculation bubble at the downstream of the bend. Comparison with results obtained by Zhang and Pothérat [9] and Chung *et al.*[4]

N	Leading eigenvalue, $\lvert\mu\rvert$	Relative error
4	0.9941048	0.0143794%
5	0.9942509	0.0003180%
6	0.9942458	0.0001927%
7	0.9942469	0.0000837%
8	0.9942477	-

Table 1: Dependence of leading eigenvalues on polynomial order. Parameter N indicates the independent polynomial order of the base flow. Leading eigenvalues computed on the mesh at $Re = 500$, $\beta = 1$ and spanwise wavenumber $k = 6.4$ are provided. The relative error is to the highest polynomial order case ($N = 8$). Given eigenvalues are real.

Table 1 depicts the accuracy of the eigenvalue computations as a function of element polynomial order N. The leading eigenvalue for $Re = 500$, $\beta = 1$ and $k = 6.4$ is real and linearly stable. The eigenvalue has converged to an absolute error of 0.0003180% at $N = 5$, relative to $N = 8$, which is of sufficient accuracy for this study. Hence, $N = 5$ is used throughout this study.

Results

Leading Eigenvalues

Figure 3 shows the the growth rates as a function of the Reynolds number and spanwise wavenumber k. Two local maxima are observed in the leading branch of each Re case: one located at low spanwise wavenumbers ($k \approx 0.3$), and the second one is at higher spanwise wavenumbers ($2 \leq k \leq 4$). The maximum σ at low k does not become positive in the range of Reynolds number studied here. However, the maximum at higher k becomes positive starting from $Re \approx 400$. Between these two local maxima, there are complex-conjugate eigenvalues over a small range of k. Larger wavenumbers than those shown in figure 3 have been studied, but all are stable and show a monotonic decrease with increasing k.

The primary linear instability occurs very close to $Re = 400$. A three-dimensional instability mode with a spanwise wavenumber of $k \approx 2$. An interpolation process was used to determine the Re and k corresponding to maximum growth rate of $\sigma = 0$. The analysis determined these conditions to be $Re_c = 397$ and

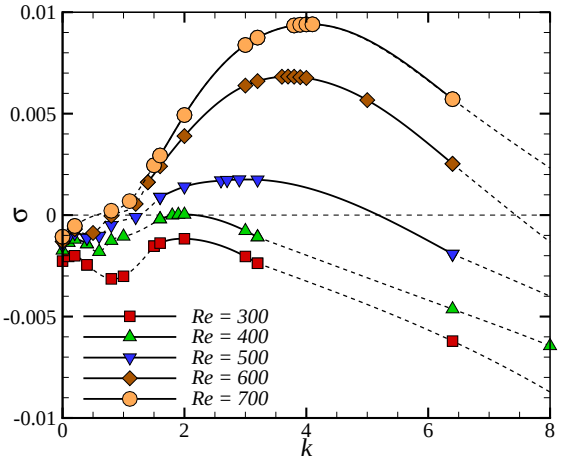

Figure 3. Growth rates as a function of spanwise wavenumber for $Re \leq 700$ (700 is included) and $\beta = 1$. Solid lines represent real eigenvalues, while dashed lines represent complex eigenvalues.

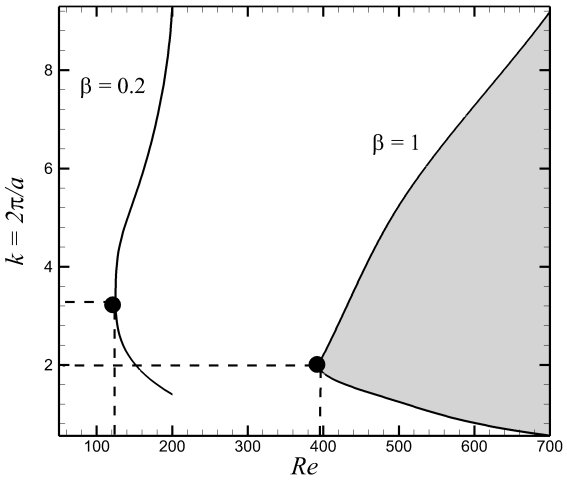

Figure 4. Neutral stability curves for sharp 180-degree bend flow with $\beta = 0.2$ and $\beta = 1$. Regions on the right of the curves represent flow conditions that are linearly unstable to three-dimensional perturbations for that particular β. The black dots represent the critical Reynolds number for each β. The critical Reynolds number for $\beta = 0.2$ is significantly lower than for $\beta = 1$

$k_c = 2$. The critical spanwise wavelength is $2\pi/k_c = 3.1a$.

Figure 4 illustrates the neutral stability curve for the sharp 180-degree bend steady flow. Flow conditions in the shaded region has at least one positive eigenvalue, and therefore is linearly unstable to three-dimensional perturbations. Flow conditions outside of this region are considered stable. The neutral curve was obtained by determining the wavenumbers corresponding to zero growth rate for each Re (Figure 3)

Figure 5 shows growth rates computed with gap ratio $\beta = 0.2$. Strong instability is observed at $Re = 200$, which is well below the threshold of $Re_c = 397$ found for the bend with $\beta = 1$. Interpolation of the local maxima in the σ-k curves suggests

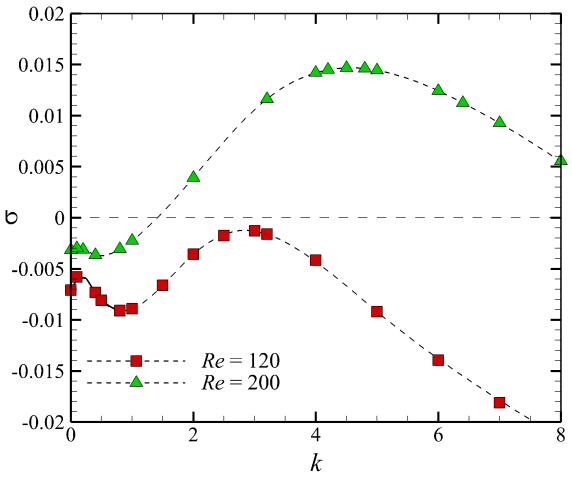

Figure 5. Growth rates for sharp 180-degree bend steady flow, $120 \leq Re \leq 200$, $\beta = 0.2$. Solid lines represent real eigenvalues, while dashed lines represent complex eigenvalues.

instability will occur just beyond $Re \approx 125$ with a spanwise wavenumber $k \approx 3$ (Figure 4). This is higher than the critical wavenumber found at $\beta = 1$, meaning that the critical spanwise wavelength is smaller at $\beta = 0.2$ than at $\beta = 1$.

Leading Eigenmodes

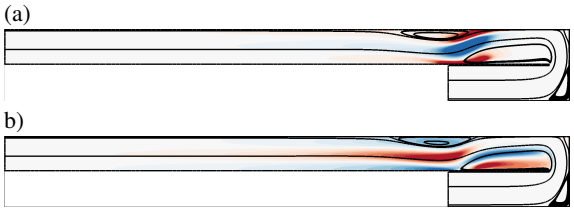

Figure 6. Streamlines of steady flow and spanwise vorticity contour of perturbation field for leading eigenvalue (a) $Re = 400$, $k = 0.2$ and (b) $Re = 400$, $k = 2$.

Figure 6 shows the streamlines of steady flow superimposed with spanwise vorticity contours of the leading eigenmodes at $Re = 400$, $\beta = 1$. These eigenmodes illustrate the structure of the linear mode that destabilises the two-dimensional base flow. Figure 6(a) evidently shows that the instability structures focused on the jet flow squeezing between the downstream end of the first bubble and the upstream end of the second bubble which is similar with the classical Taylor–Görtler instability because the main flow in between the bubbles is subject to destabilizing concave curvature [5]. In Taylor–Görtler instability, vortices are aligned with the flow direction with adjacent recirculation bubbles rotating in opposite senses. However, this eigenmode does not give positive growth rate in the range of steady-state two-dimensional base flow Reynolds number. At higher spanwise wavenumber (Figure 6(b)), there are strong perturbation structures aligning with the jet passing the second recirculation bubble in addition to the perturbation structures in the first bubble. This mode of instability gives positive growth rate at $Re \geq Re_c$.

Conclusions

This study has shown that the two-dimensional base flow around a sharp 180-degree bend exhibits a synchronous three-dimensional instability starting from a certain value of Reynolds number when perturbed with an infinitesimal perturbation at a range of wavenumber. The critical Reynolds number and the three-dimensional instability spanwise wavelength for an opening ratio of $\beta = 1$ have been precisely calculated and found to be $Re_c = 397$ and $\lambda_c = 3.1$ in non-dimensional unit based on maximum inlet velocity U_o and inlet height a. A lower β case demonstrated an instability occurring at a lower Re_c which may be explained by the dynamics of the jet generated by the very small bend opening. This study was the first to elucidate the linear stability of these flows and the results have provided a useful platform for future numerical work concerning transient growth analysis and analogous flows in heat exchanger applications.

Acknowledgements

This research was supported by ARC Discovery Grant DP120100153, high-performance computing time allocations from the National Computational Infrastructure (NCI) and the Victorian Life Sciences Computation Initiative (VLSCI), and the Monash SunGRID. A.M.S. is supported by Ministry of Education Malaysia and International Islamic University Malaysia.

References

[1] Barkley, D., Gomes, M. G. M. and Henderson, R. D., 2002, Three-dimensional instability in flow over a backward-facing step, *Journal of Fluid Mechanics*, **473**, 167–190.

[2] Blackburn, H., Sherwin, S. J. and Barkley, D., 2008, Convective instability and transient growth in steady and pulsatile stenotic flows, *Journal of Fluid Mechanics*, **607**, 267–277.

[3] Boccaccini, L., Giancarli, L., Janeschitz, G., Hermsmeyer, S., Poitevin, Y., Cardella, A. and Diegele, E., 2004, Materials and design of the european demo blankets, *Journal of Nuclear Materials*, **329**, 148–155.

[4] Chung, Y. M., Tucker, P. G. and Roychowdhury, D., 2003, Unsteady laminar flow and convective heat transfer in a sharp 180 bend, *International journal of heat and fluid flow*, **24**, 67–76.

[5] Ghia, K., Osswald, G. and Ghia, U., 1989, Analysis of incompressible massively separated viscous flows using unsteady navier–stokes equations, *International Journal for Numerical Methods in Fluids*, **9**, 1025–1050.

[6] Karniadakis, G. E., Israeli, M. and Orszag, S. A., 1991, High-order splitting methods for the incompressible navier-stokes equations, *Journal of computational physics*, **97**, 414–443.

[7] Kleinhans, M. G., Blanckaert, K., McLelland, S. J., Uijttewaal, W. S., Murphy, B. J., van de Kruijs, A. and Parsons, D., 2010, Flow separation in sharp meander bends, in *HYDRALAB III Joint User Meeting*.

[8] Thomson, J., 1876, On the origin of windings of rivers in alluvial plains, with remarks on the flow of water round bends in pipes, *Proceedings of the Royal Society of London*, **25**, 5–8.

[9] Zhang, L. and Pothérat, A., 2013, Influence of the geometry on the two-and three-dimensional dynamics of the flow in a 180 sharp bend, *Physics of Fluids*, **25**, 053605.